Journal of *Marine Science and Engineering*

MDPI

Article

Experimental Scours by Impinging Twin-Propeller Jets at Quay Wall

Yonggang Cui [1], Wei Haur Lam [1,*], Zhi Chao Ong [2], Lloyd Ling [3], Chee Loon Siow [4], Desmond Robinson [5] and Gerard Hamill [5]

1 State Key Laboratory of Hydraulic Engineering Simulation and Safety, Tianjin University, Tianjin 300350, China; cui_yonggang@tju.edu.cn
2 Department of Mechanical Engineering, Faculty of Engineering, University of Malaya, Kuala Lumpur 50603, Malaysia; alexongzc@um.edu.my
3 Department of Civil Engineering, Lee Kong Chian Faculty of Engineering and Science, Universiti Tunku Abdul Rahman, Kajang 43000, Malaysia; linglloyd@utar.edu.my
4 Department of Aeronautical, Automotive and Ocean Engineering, Universiti Teknologi Malaysia, Johor Bahru 81310, Malaysia; scloon@mail.fkm.utm.my
5 School of Natural and Built Environment, Architecture, Civil & Structural Engineering and Planning, Queen's University Belfast, David Keir Building, Stranmillis Road, Belfast BT9 5AG, UK; Des.robinson@qub.ac.uk (D.R.); g.a.hamill@qub.ac.uk (G.H.)
* Correspondence: wlam@tju.edu.cn

Received: 20 September 2020; Accepted: 20 October 2020; Published: 2 November 2020

Abstract: Experiments were conducted to investigate the seabed scour holes due to the interaction between the twin-propeller jet and quay wall. Vertical quay wall was modelled by using a polyvinyl chloride (PVC) plastic plate in a water tank. The relationship between the positions of the propeller and the vertical quay wall was designed according to the actual working conditions of a ship entering and leaving a port. Propeller-to-wall distance and rotational speed were changed to observe the various scour conditions. The scour depth was measured by using an Acoustic Doppler Velocimeter (ADV). Primary scour hole was found within the jet downstream and secondary scour hole occurred beneath of the propeller. Third scour hole was found close to the quay wall due to horseshoe vortices. The maximum scour position of this third scour hole was found at the jet centre near the quay wall. Temporal formation of scour holes can be divided into three stages: axial scour formation, obstructed scour expansion and equilibrium stages. The quantitative relationships for six characteristic parameters of the scour pit were established including the maximum scour depth ($\varepsilon_{max,q}$), maximum scour depth position ($X_{m,q}$), maximum scour width ($W_{m,q}$), length of main scour pit ($X_{S,q}$), maximum deposition height ($Z_{D,q}$), and location of maximum deposition height ($X_{D,q}$).

Keywords: twin-propeller; propeller jet; scour; quay wall

1. Introduction

The carrying capacity and high-speed performance of ships are increasing with the development of the marine economy and trade. When a ship is fully loaded, the channel depth significantly limits the selection of the ship navigation route. Typically, a distance between the waterway seabed and the ship keel is available to prevent a ship grounded. However, the clearance is sometimes insufficient to dissipate the kinetic energy from the high-speed propeller jet or the complicated twin-propeller jets compared to the single-propeller ship. The high-speed jet is spreading to reach the bottom of the hydraulic structures in ports and docks. The jet velocity can reach several meters per second, which may induce unpredictable scour damage to the river channel and waterways.

Propeller scouring received attentions for decades with initial consideration by using the plain water jet. Albertson et al. [1] proposed the theoretical works to enable the velocity prediction within the jet from an orifice by using the axial momentum theory and Gaussian normal distribution. The followers borrowed the theoretical equations to establish the propeller jet theory. Blaauw and van de Kaa [2], Berger et al. [3], and Verhey et al. [4] analysed the three-dimensional characteristics of a propeller jet. Hamill [5] used a pitot tube to measure the flow field in a single-propeller jet and established the jet structure of the single propeller. Lam [6] proposed a semi-empirical model based on the axial momentum theory. Laser Doppler Velocimetry (LDA) and Computational Fluid Dynamics (CFD) correction were applied to provide corrections for a wider range of cases. The research methods on propeller jets mainly included the numerical simulations and model tests. Du et al. [7], Su et al. [8], and Hong et al. [9] analysed the mesh models using the numerical method and evaluated the hydrodynamic performance characteristics of the models. Previous studies were mainly focused on single-propeller ships. Jiang et al. [10] developed a twin-propeller model and simulated the jet flow field of the twin-propeller using a standard k–ε model to predict the distribution of twin-propeller-jet flow field.

Propeller scour is another crucial research topic for engineering safety. BAW [11] and PIANC [12] provide guidance for the protection of berthing structures from ship scour. Bergh and Cederwall [13,14], Verhey [15], Hamill [5], Stewart [16], Kim et al. [17], and McGarvey [18] evaluated the effect and scoured damage of ship propeller jets under the influence of traditional hydraulic structures. Hamill et al. [19] investigated the scour formation of a propeller jet without sidewall restriction and restricted the jet using a quay wall. Hamill et al. focused on the analysis of different scour processes at different distances from the quay wall to the propeller jet and derived an expression for estimating the variation in the maximum scour depth during final scouring. Hong et al. [20], Wei and Chiew [21], and Wei et al. [22] examined local scour pits near the toe of a slope. They found that the maximum scour depth initially increases and then decreases with the toe clearance (longitudinal distance between the propeller and wall) until the wharf effect is no longer significant. Tan et al. [23] carried out an experimental study on the local scour caused by a propeller when the quay wall is a closed berth structure. The changes in scouring with time at different propeller clearances, propeller speeds, and distances from the propeller surfaces were analysed in their study, and a new empirical equation was proposed to determine the scour depth. Cui et al. [24] derived an equation for predicting the scour depth of a twin-propeller through dimensional analysis considering the diameter and speed of the twin-propeller and found that the twin-propeller scour consisted of large and small scour pits and sedimentary dunes. The prediction method of the twin-propeller scour, and the entire section was based on normal Gaussian distribution. Mujal-Colilles et al. [25], Yuksel et al. [26], and Yew [27] evaluated the scour of a no-quay wall through twin-propeller slurry tests.

To date, research on the scour of twin propellers in different rotation directions near a quay wall has not been investigated in detail. In this study, based on a previous experimental study of a single propeller combined with three-dimensional printing technology, the scouring of a vertical quay wall induced by a twin-propeller jet was investigated using an acoustic Doppler velocimeter (ADV). Physical model tests of twin propeller scouring were performed in the laboratory. The scour simulation of ships used in practical engineering, especially the most common vertical port structure, was conducted.

2. Experimental Method

2.1. Experimental Setup

Based on the operational requirements and natural conditions of different ports, common wharf structures can be divided into gravity, high pile, and sheet pile types. The main functions of wharves include providing access for ships to stop, load, and unload cargo and passengers. Currently, the most widely used wharf structure is the vertical wharf, which is convenient for ships to dock and machinery

to drive to the wharf front directly. The use of vertical wharf improves loading and unloading efficiency. Most previous studies on scouring were focused on the vertical wharf structure.

By using a case study of undisclosed actual port, the vertical height of the vertical port is 8.2 m, the upper part of the water line is 2.2 m high, and the water depth is 6 m. When the ship berths, the maximum depth of the propeller shaft from the horizontal plane is 3.5–5 m, which is perpendicular to the vertical quay wall. In this study, the scouring process of a ship propeller was simulated in the laboratory. The simulation device was set up in the static water tank of the Marine Renewable Energy Laboratory of Tianjin University (Figure 1). The surface of the polyvinyl chloride (PVC) baffle was sprayed with white pigment. When the pigment was air-dried thoroughly, the surface was smeared with sand to roughen it and simulate the surface roughness of the vertical wharf. A sand bed of 0.1 m height was evenly laid at the bottom of the tank to replicate the sediments at the bottom of the port. The baffle was vertically positioned in and out of the sand bed and fixed. After the impoundment was completed, the depth and width from the sand bed to the water surface were 0.3 and 0.7 m, respectively, to ensure that the jet of the twin-propeller could be sufficiently diffused in the baffle plane.

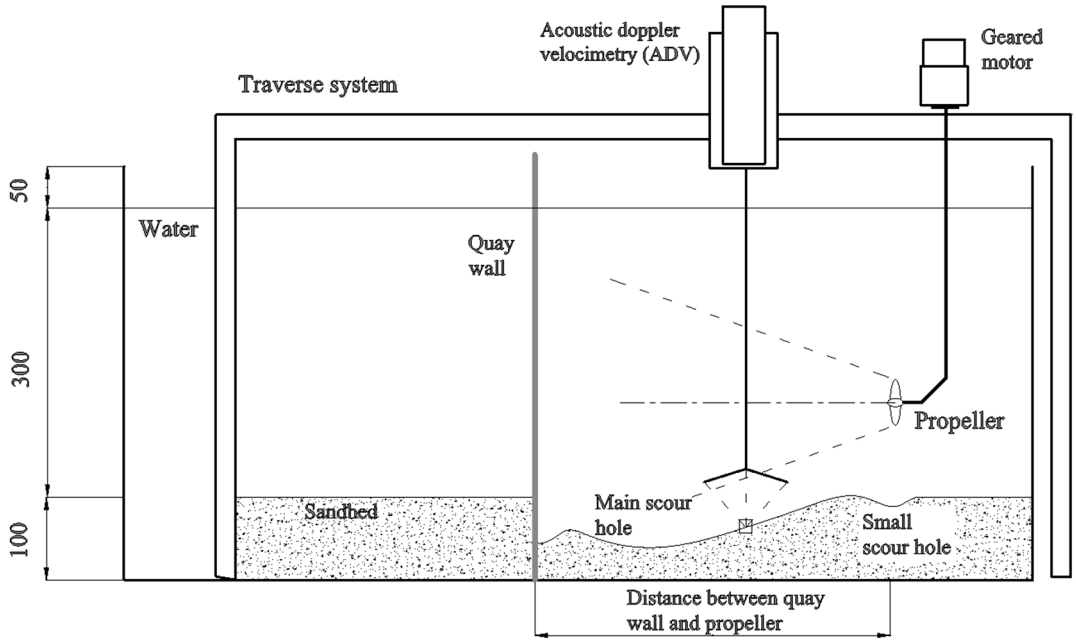

Figure 1. Experimental setup.

The selected distances between propeller and vertical quay wall is based on Hamill et al. [19]'s research. The distances are set to 350 mm, 500 mm, 900 mm, 1250 mm, 1500 mm, and 1800 mm (2-14D_p). Li et al. [28] suggested that scour beneath a twin pipeline system with various distances. Smaller horizontal gap ratios will suppress the vortex, result in delayed scour beneath the downstream pipeline. A short distance ($2D_p$) and long distance ($9D_p$) scouring tests are designed in original experimental design. No deeper scour pit was found at a shorter distance. The surrounding sand returns to the scour pit after scouring process. For a long distance ($9D_p$), the scour pit is unobvious near the quay wall. The experimental distance of 3-7D_p was chosen for the measurements. The clearance effect was reported in the works such as Ong et al. [29]. The distance between propeller and sand bed was set same to Cui et al. [30] without quay wall.

Previous studies on propeller scouring show that propeller jets can be classified as a type of nonuniform flow. The Reynolds number of particles is related to the fluid velocity near the sand layer. Sea sand was used to simulate the seabed environment. The sand density was 2650 kg·m^{-3} with a median sediment size of d_{50} = 0.2 mm. The sediment size was estimated using a standard particle. The sand was homogenous based on the geometric standard deviation ($\sqrt{d_{84}/d_{16}}$) value of

1.4 according to the cumulative frequency curve of sand particle size distribution, as shown in Figure 2 (Cui et al. [24]).

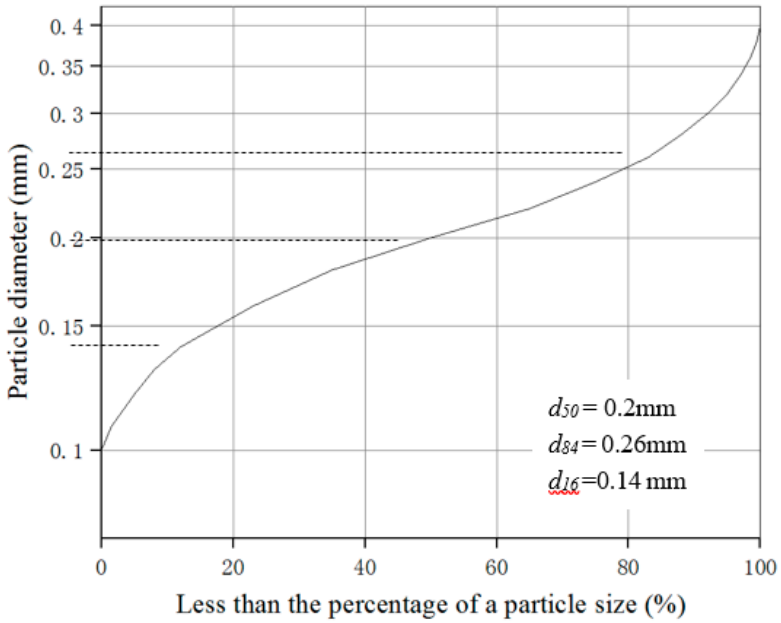

Figure 2. Cumulative frequency curve of sand particle size distribution (Cui et al. [24]).

2.2. Scaling Effects

Hamill et al. [19] proposed the empirical model to predict the single propeller induced scour in sandbed with fine and coarse sediments. The maximum scour depth of single-propeller scour (ε_m) can be related as a function in Equation (1).

$$\varepsilon_m = f\left(V_0, D_p, d_{50}, C, \rho, g, \Delta\rho, \nu\right) \tag{1}$$

where V_0 is the efflux velocity (m/s); d_{50} is the median sediment grain size (m); D_p is the propeller diameter (m); C is the clearance distance between the propeller tip and the seabed (m); ρ is the density of fluid (kg/m^3); $\Delta\rho$ is the difference between the mass density of the sediment and the fluid (kg/m^3); g is the acceleration due to gravity (m/s^2); and ν is the kinematic viscosity of fluid (m^2/s). The efflux velocity can be calculated using Equation (2).

$$V_0 = 1.59 n D_P \sqrt{C_t} \tag{2}$$

where n is the rotational speeds (rad/s), and C_t is the propeller thrust coefficient.

Reynolds numbers of propeller and jet are examined to satisfy the common requirement for scaling effects using Equations (3) and (4).

$$R_{flow} = \frac{V_0 D_P}{\nu} \tag{3}$$

$$R_{prop} = \frac{n L_m D_p}{\nu} \tag{4}$$

where, D_p is the diameter of the propeller (m); ν is the kinematic viscosity of the fluid (8.54×10^{-7} m^2 /s) at 27 °C; n is the number of rotation speed per second. Blaauw and van de Kaa [2] defined the length of a propeller L_m in Equation (4) as Equation (5).

$$L_m = \beta D_p \pi \left[2N \left(1 - \frac{D_h}{D_p} \right) \right]^{-1} \tag{5}$$

where, D_h is the diameter of the hub (m); N is the number of blades and β is the blade area ratio (Blade area ratio is an indicator to determine the solidity of blade to the circular area of the propeller).

From C_t = 0.4, D_h = 11.5 mm, D_p = 55 mm, β = 0.473, N = 3, the calculated L_m is 1.840 and V_0 is 0.463 m/s. The calculation of Reynolds number for propeller is 7.4×10^5 and Reynolds number of jets is 2.23×10^4. Blaauw and Van de Kaa [2] and Verhey [4] proposed that the scaling effect could be neglected at high Reynolds numbers. The calculated Reynolds numbers of jets were all greater than 3×10^3. The scaling effect caused by the kinematic viscosity of water can be neglected.

Verhey et al. [4] provided a design criterion for physical model of propeller jet experiments. Considering the size factor, the Froude number (F_0) is considered as a very important reference factor in the previous studies of circular jet and propeller jet scouring, which is defined as Equation (6).

$$F_0 = \frac{V_0}{\sqrt{g d_{50} \frac{\Delta \rho}{\rho}}} \tag{6}$$

where d_{50} is the median sediment grain size (m); ρ is the density of fluid (kg/m^3); $\Delta\rho$ is the difference between the mass density of the sediment and the fluid (kg/m^3); g is the acceleration due to gravity (m/s^2). The calculated F_0 in this study is 8.135. Hong et al. [9] suggested that a range of $5.55 < F_0 < 11.1$ for their experiments.

2.3. Selection of Measurement Position and Method

In the twin-propeller simulation system, two propeller models of the same type but in opposite directions were used. The distance between the two propellers was $2D_p$, where D_p is the diameter of the propeller. The height between the blade tip of the twin-propeller and the sand bed bottom was maintained as $0.5D_p$ by adjusting the height between the horizontal support and telescopic shaft. The distances between the propeller outflow plane and vertical baffle were set to $3D_p$, $5D_p$, and $7D_p$. When the distance exceeded $7D_p$, the scour strength decreased significantly. The rotating state of the ship was simulated at 500 rpm using the twin propellers. Two-hour scouring tests were performed on the internal and external twin propellers using the steering control switch. The overall test setup is described in Table 1.

Table 1. Scouring test of quay wall.

Data Set.	T	Propeller	n (rpm)	D_p (mm)	d_p (mm)	d_q (mm)
1	2 d	ECRTP	500	55	$2D_p$	$3D_p$
2	2 d	ICRTP	500	55	$2D_p$	$3D_p$
3	2 h	ECRTP	500	55	$2D_p$	$5D_p$
4	2 h	ICRTP	500	55	$2D_p$	$5D_p$
5	2 h	ECRTP	500	55	$2D_p$	$7D_p$
6	2 h	ICRTP	500	55	$2D_p$	$7D_p$

Six sets of experimental groups were constructed to determine the scouring mechanisms of external counter rotating twin-propeller (ECRTP) and internal counter rotating twin-propeller (ICRTP) (Table 1). Measurements for the six experimental sets included (1) external rotating twin-propeller scour with $3D_p$ quay wall spacing, (2) internal rotating twin-propeller scour with $3D_p$ quay wall spacing, (3) external rotating twin-propeller scour with $5D_p$ quay wall spacing, (4) internal rotating

twin-propeller scour with $5D_p$ quay wall spacing, (5) external rotating twin-propeller scour with $7D_p$ quay wall spacing, and (6) internal rotating twin-propeller scour with $7D_p$ quay wall spacing.

A group of points was recorded on the measurement grid along both axis directions or transverse intervals to obtain the maximum depth (Table 2). For experimental set 1, 11 temporal measurements were performed for periods of 5 min, 10 min, 20 min, 30 min, 1 h, 2 h, 4 h, 8 h, 12 h, 1 d, and 2 d. Seventeen spatial measurement points were selected along the rotation axis of the right propeller from the aft view with a grid of 10 mm. The measurement points were extended 30 mm at a right angle along the transverse interval. Similar parameters were adopted for experimental set 2. For the other experimental sets, the temporal measurements were taken for 5 min, 10 min, 20 min, 30 min, 1 h, and 2 h.

Table 2. Measurement position.

Data Set.	*T*	Position	Point Selection
1	5 m, 10 m, 20 m, 30 m, 1 h, 2 h, 4 h, 8 h, 12 h, 1 d, 2 d	Two axis directions	17 points with 10 mm grid from efflux plane up to 170 mm ($3D_p$) downstream
		Transverse interval distribution	Varies with the transverse range of scouring (at an interval of 30 mm), 57 points at the widest position of scouring
2	5 m, 10 m, 20 m, 30 m, 1 h, 2 h, 4 h, 8 h, 12 h, 1 d, 2 d	Two axis directions	17 points with 10 mm grid from efflux plane up to 170 mm ($3D_p$) downstream
		Transverse interval distribution	Varies with the transverse range of scouring (at an interval of 30 mm), 57 points at the widest position of scouring
3	5 m, 10 m, 20 m, 30 m, 1 h, 2 h	Two axis directions	30 points with 10 mm grid from efflux plane up to 300 mm ($5D_p$) downstream
		Transverse interval distribution	Varies with the transverse range of scouring (at an interval of 30 mm), 54 points at the widest position of scouring
4	5 m, 10 m, 20 m, 30 m, 1 h, 2 h	Two axis directions	30 points with 10 mm grid from efflux plane up to 300 mm ($5D_p$) downstream
		Transverse interval distribution	Varies with the transverse range of scouring (at an interval of 30 mm), 65 points at the widest position of scouring
5	5 m, 10 m, 20 m, 30 m, 1 h, 2 h	Two axis directions	39 points with 10 mm grid from efflux plane up to 390 mm ($7D_p$) downstream
		Transverse interval distribution	Varies with the transverse range of scouring (at an interval of 30 mm), 54 points at the widest position of scouring
6	5 m, 10 m, 20 m, 30 m, 1 h, 2 h	Two axis directions	39 points with 10 mm grid from efflux plane up to 390 mm ($7D_p$) downstream
		Transverse interval distribution	Varies with the transverse range of scouring (at an interval of 30 mm), 60 points at the widest position of scouring

3. Scour Near Vertical Quay Wall

3.1. Temporal Scour Process

Most scholars investigated the observation time of small-scale model tests in previous studies. In this study, the long-term scour structure variations based on experimental sets 1 and 2 were recorded (Table 3). The distance between the propeller outflow plane and vertical quay wall was $3D_p$. Compared with the experimental setup of $5D_p$ and $7D_p$, the propeller jet velocity was higher, and the fluctuation was more significant. The entire scour structure was evaluated and measured after 5 min, 10 min, 20 min, 30 min, 60 min, 2 h, 4 h, 8 h, 12 h, 24 h, and 48 h. Within the first 5 min, two large scour pits, which were produced by the external and internal rotating twin propellers, were formed near the quay wall. The maximum scour depth was located in the axial direction of the two propellers. The formation of the sandpit was not mainly owing to the axial movement of the jet but by the backflow formed by the jet impinging on the quay wall. From 5 min to 2 h, the sandpit gradually deepened, and the transverse range increased significantly. Visible sand deposition peaks were observed around the sandpit. Two maximum scour depths existed near the quay wall, and the scour depth between the two propeller axes was close to the maximum axial depth. The maximum scour depth was only along the central axis of the two propellers. At the bottom of the quay wall, the sand particles around the wall rolled up the sand particles at the sandpit bottom in a vortex form, and the sandpit particles were thrown up to the slope of the sandpit. The sand particles on the slope of the sandpit filled up the

sandpit, which had only been rolled up under the action of gravity, and the sandpit particles reached the dynamic equilibrium state.

Table 3. Scouring process.

T (min\h\d)	ECRTP	ICRTP
5 min		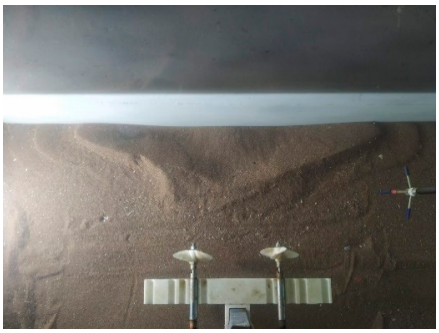
10 min		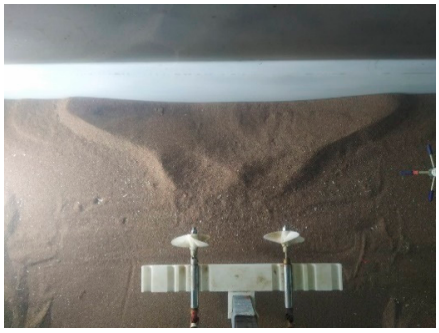
20 min		
30 min		

Table 3. *Cont.*

T (min\h\d)	ECRTP	ICRTP
60 min		
2 h		
4 h		
8 h		

Table 3. *Cont.*

T (min\h\d)	ECRTP	ICRTP
12 h		
1 d		
2 d		

The shear stress of fluid on sediment is related to fluid velocity. The propeller jet is a complex non-uniform rotating flow. The propeller jet has not only axial motion, but also tangential and radial motions. The process of sediment movement is complex and the formation of scour pits is influenced by the complicated process of shear stresses and turbulent intensities. In the initial stage of scour, the high-speed jet in vertical direction is produced when being blocked by quay wall. The movement of sediment with jet can be regarded as suspended movement. The sediment returns to the surface of sand bed again with the reduction of jet velocity.

When the propeller jet diffuses to the sand bed surface, the sand particles on the bed will be subjected to shear forces. It is characterised by drag force and lifting force. The shear stresses of sand particles are directly related to the position and jet velocity. The cohesive force between sediment particles will resist the shear force. When the jet velocity is high enough, the shear stress on the sand bed surface is far greater than its cohesive force. The sand movement becomes more intense. The shear stresses are close to the cohesive force with reduction of jet velocity. When the surface velocity continues to decrease, the shear stresses of the sediment are less than the cohesive force and the sediment no longer moves.

Set 1 and Set 2 were used as examples, and the scour depth at each time point was recorded. The changes in the axial scour depth of the two propellers and the lateral scour depth near the quay

wall were recorded using the ranging function of the ADV. It was found that the maximum scour depth varied with time (Figure 3). The maximum scour depth of the external twin-propeller was located on the two propeller axes, and that of the internal rotating twin-propeller was on the central axis. Generally, the maximum scour depth of the two propellers were almost equal. After 4 h, the scour depth reached 48 mm, which was approximately 87% of the final scour depth. After 8 h, the scour depth was approximately 49 mm. It was considered that the dynamic equilibrium stage was reached when the scouring time was 4 h.

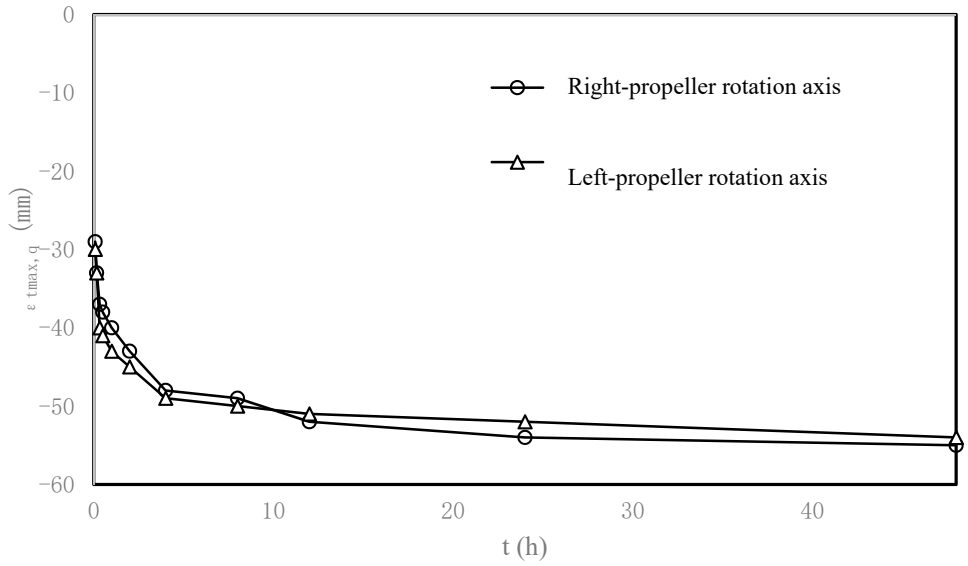

Figure 3. Relationship between temporal scour depth and scour time.

3.2. Scouring Stages for Twin Propellers

The unlimited scour process of the twin propellers could be divided into three stages: (1) independent stage, (2) merging stage, and (3) establishment stage. The independent scouring stage only initially occurred for a short period, but this stage was not observed during the scouring tests for the vertical quay wall. The jets of the two propellers merged from the time the twin propellers were operated, which resulted in scouring damage to the sand bed. The scouring of the vertical quay wall could also be divided into three stages, as follows.

(1) Axial scour formation

During the initial scouring stage, the twin-propeller jets diffused along the axial direction downstream. The jets carried sand particles on the sand bed surface downstream until the sand particles reached near the quay wall. The duration of this process was short and influenced by the distance between the twin propellers and quay wall.

(2) Obstructed scour expansion

Near the quay wall, the jet diffused in a plane owing to the blocking effect of the quay wall. The jet velocity was sufficient to continue transporting the sand particles near the quay wall to both sides. From upstream of the quay wall to the propeller outflow plane, the jet was also blocked. The jet moved irregularly to both sides, which resulted in the lateral formation of the scour pit. This process lasted for a long time and occurred from the jet to the quay wall until the scour pit stopped expanding significantly.

(3) Equilibrium stage

Near the quay wall, the jet diffused in the plane of the quay wall and formed a vortex at the junction between the sand bed and quay wall. The vortex pushed the sand particles backward from the quay wall upstream across a short distance (approximately 30–40 mm). Subsequently, the sand particles settled at this distance range to form a local deposition peak. Under the action of gravity,

the collapsed sand particles were still transported by the vortex and returned to the deposition peak in the reverse direction. Thus, the cycle occurred continuously.

3.3. Scour Patterns between the External-Rotating and Internal-Rotating Systems

Cui et al. [30] reported that the scour structures of internal and external rotating twin propellers without considering the effect of the quay wall were different. The jets of the internal and external rotating twin propellers formed tangential downward and upward jet components, respectively, on the symmetric plane downstream of the propellers. The tangential downward jet caused the maximum scour depth to exist on the symmetric plane of the two propellers. The tangential jet component caused the scour of the external twin-propeller to form a ridge-like scour pit on the symmetry plane. The maximum scour depth was located on the rotation axis of the two propellers.

It is also observed during the experimental tests of the twin-propeller that scours were formed owing to the influence of the vertical quay wall. For Sets 5 and 6, the distance between the twin propellers and quay wall was $7D_p$ (Figure 4). The twin-propeller jet impinged on the vertical quay wall and diffused at approximately 40 mm near the quay wall, and thus, formed a large local scouring zone at the quay wall bottom. Between the scour zone and propeller outflow plane, the scour structure was analogous to that without a quay wall. The maximum scour depth of the internal rotating twin propellers existed on the central axis. In contrast, external rotating twin propellers existed on the rotating axis of the propeller.

Figure 4. ICRTP and ECRTP wall scour structures.

In this study, the scour structures under the action of vertical baffles were divided into three parts: small scour pit, main scour pit, and local scour zone near the quay wall (Figure 5). This classification was made to distinguish different scour structures with or without vertical baffles. There is a vertical vortex around the propeller. The formation of the vertical vortex is caused by the disturbance of the propeller blade and appears under the propeller. A small circular scour pit appears in the sand bed under the propeller.

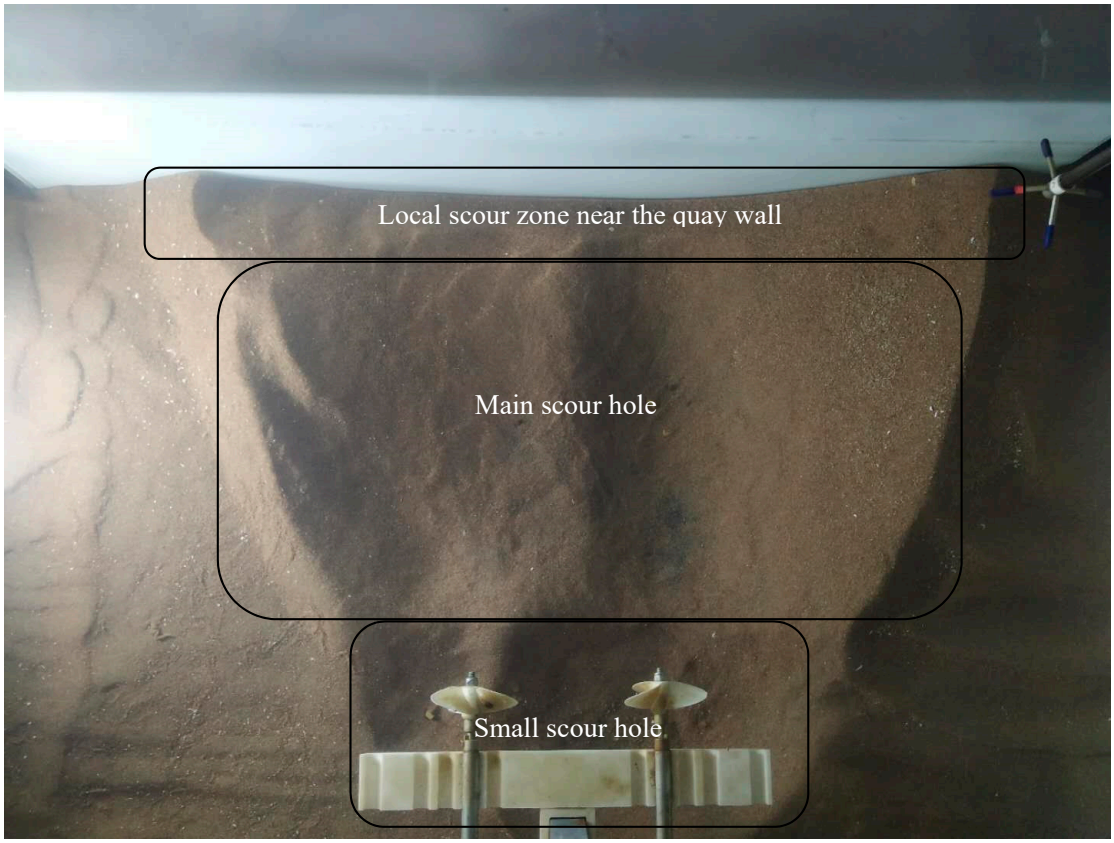

Figure 5. Scour structures of twin propellers under quay wall effect.

4. Maximum Scour Depth of Twin Propellers Influenced by Quay Wall

4.1. Comparison of Scour Depth between Free Twin Propeller and Quay Wall

Cui et al. [30] found that a twin-propeller without a quay wall scours into three structures: small scour pits, large scour pits, and scour deposits. The maximum scour depth was in the middle of the large scour pit. Differences between the internal and external rotating propellers at the transverse position of the maximum scour depth were observed. The maximum scour depth could be predicted using Equations (7)–(9).

$$\varepsilon_{\text{twin}} = \Omega_t [ln(t)]^{\Gamma_t} \tag{7}$$

$$\Omega_t = 0.2526 \times \left(\frac{d_p}{d_{50}}\right)^{-0.859} \left(\frac{C}{d_{50}}\right)^{-4.63} \left(\frac{D_p}{d_{50}}\right)^{3.58} {F_0}^{4.535} \tag{8}$$

$$\Gamma_t = 1.389 \times \left(\frac{d_p}{d_{50}}\right)^{0.1571} \left(\frac{C}{d_{50}}\right)^{0.742} \left(\frac{D_p}{d_{50}}\right)^{-0.522} {F_0}^{-0.682} \tag{9}$$

The results showed that the twin-propeller jet could not diffuse freely along the axial direction. The scour structure was influenced by the distance between the quay wall and propeller. Figure 6 shows the comparison between the axial scour depths of the scour structure under the influence of the quay wall. When the outflow plane of the internal rotating twin propellers was $3D_p$ away from the vertical baffle, the maximum scour depth measured at the outflow plane was 0–20 mm above the sand bed. The free scour without the baffle was 0–10 mm below the sand bed, which was attributed to the high-speed backflow and vortex formed by the twin-propeller jet impinging on the baffle. This was caused by the deposition of sand particles owing to the reverse movement of the entrained sand particles. When there was no baffle, the position of x = $0D_p$ was observed for the structure of the small scour pit. The scour depth should be below the sand bed. From x = $0D_p$ to

x = $3D_p$, the scour depth increased almost along the fixed slope and reached the maximum scour depth at x = $3D_p$. The maximum scour depth was located on the central axis of the two propellers, and its value was 70 mm. At a short distance (10 mm) from the downstream of $3D_p$ to the vertical baffle, the scour depth decreased, which could be attributed to the strong bond between the sand particles and baffle plate, and the jet diffusion on the baffle could not push the sand. When the effect of baffles is neglected, previous studies have shown that the maximum scour depth is approximately 41.5 mm. Hence, the barrier effect of the quay wall increased the scour depth by 68%. The maximum scour depth of the external twin-propeller increased by 56% compared with that without the quay wall effect (Figure 6b). Therefore, when the twin propellers were very close to the quay wall, the scour damage was more severe. When the distance between the twin propellers and baffle was $5D_p$ (Figures 5d and 6c), the scour depth of the twin propellers exceeded that without the quay wall, and the maximum scour depth increased by up to 24%. Figure 6e,f shows the maximum scour depth of the internal and external rotating twin propellers at $7D_p$. From the propeller outflow plane to the position of the maximum scour depth (x = $3D_p$), the scour structure with or without baffles was almost unchanged, and the maximum scour depth of the main scour pit was also almost equal. From x = $3D_p$ to x = $7D_p$, the maximum scour depth gradually increased with an increment of 20–35% under the condition of quay wall obstruction, and there was no significant sediment peak near x = $5D_p$. Thus, the scour depth continued to increase. The scour depth lies in the local scour zone near the quay wall. The maximum scour depth, in this case, was analogous to the main scour pit.

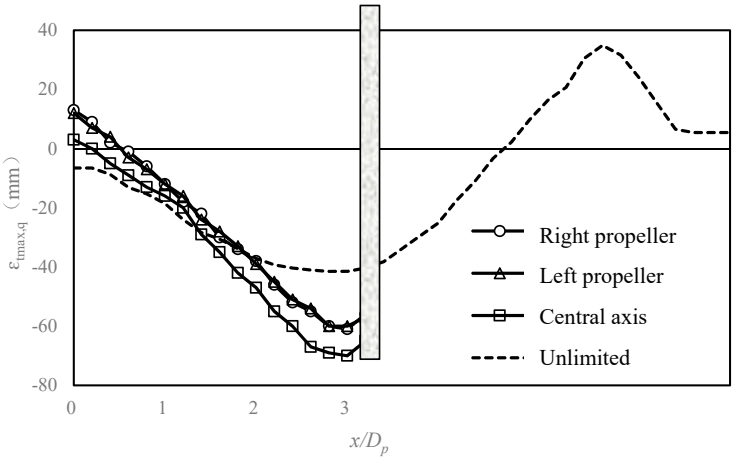

(**a**)

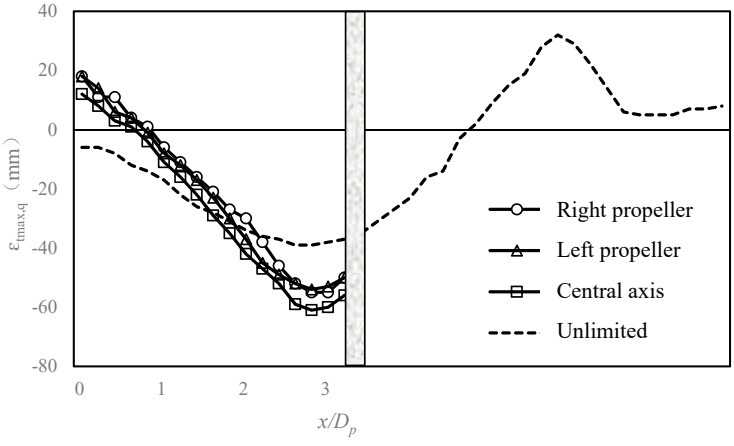

(**b**)

Figure 6. *Cont.*

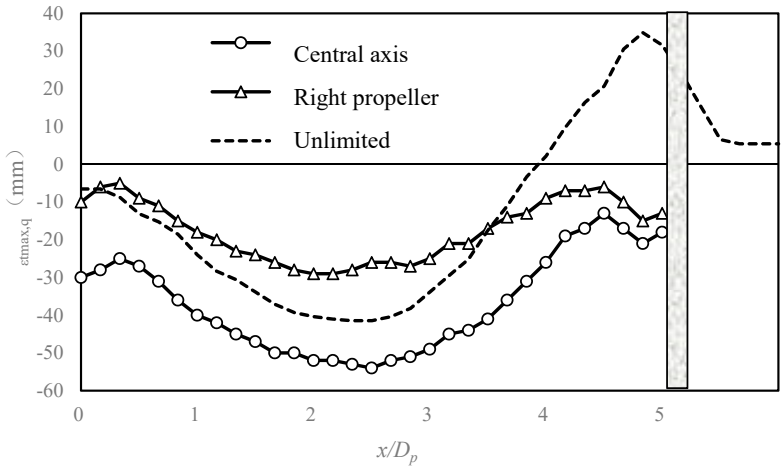

(**c**)

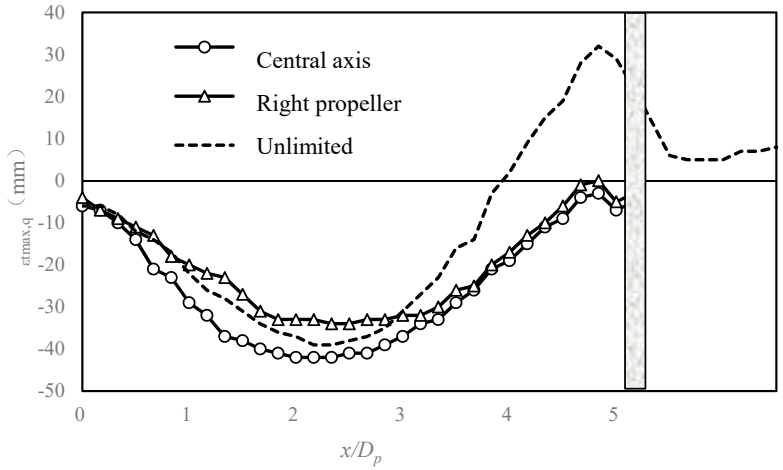

(**d**)

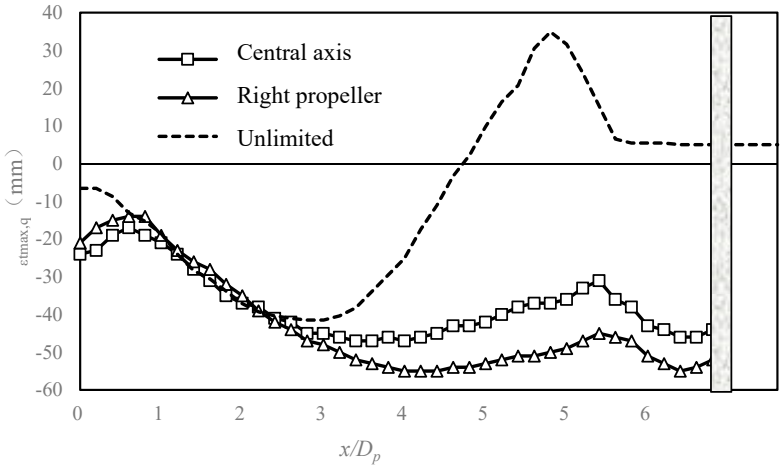

(**e**)

Figure 6. *Cont.*

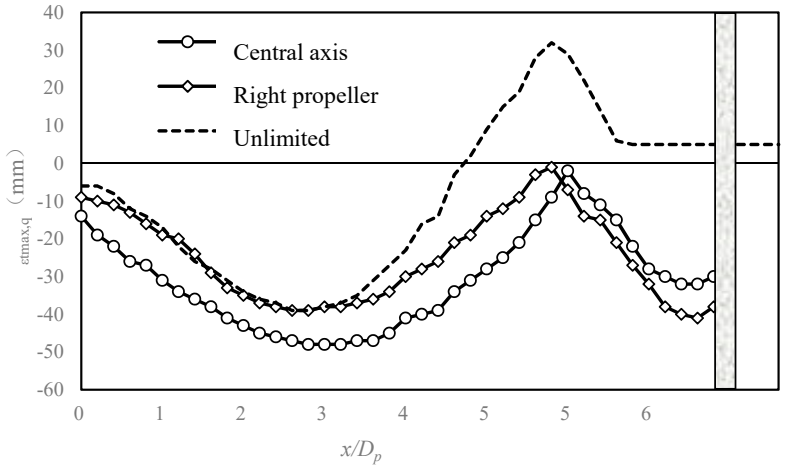

(**f**)

Figure 6. Values of axial scour depth for different propeller diameters and (**a**) ICRTP ($3D_p$); (**b**) ECRTP ($3D_p$); (**c**) ICRTP ($5D_p$); (**d**) ECRTP ($5D_p$); (**e**) ICRTP ($7D_p$); (**f**) ECRTP ($7D_p$).

In Figure 6, the test data presented in Cui et al. [30] are used for comparison because similar tests were performed using twin propellers, but the difference was that the blocking effect of the vertical quay wall was considered in this paper. However, a few research results on double-helix vertical quay wall scours are available in the literature. The author applied the scour test data of the Hamill single propeller to improve the test results (Figure 7). The maximum scour axis of each group of tests in this study was dimensionless with the unlimited scouring axis of a single propeller. The abscissa represented the dimensionless axial distance (x/D_p). When the distance from the quay wall was $3D_p$, the maximum scour depth of the inner and outer rotating twin-propeller slurries were located on the central axis near the quay wall, and the maximum scour depth axis of the Hamill single screw was also located near $3D_p$. The ratio of the maximum scour depth $\frac{\varepsilon_{tmax,q}}{\varepsilon_m}$ was approximately 2–2.3. With an increase in the distance between the twin-screw slurry and vertical quay wall, the maximum scour depth was still located at the axial distance of $3D_p$ at the position of $x/D_p = 5D_p$. Although local large scour pits were excavated near the quay wall, these pits had significantly shallower depths than the scour depth at the $3D_p$ position, and $\frac{\varepsilon_{tmax,q}}{\varepsilon_m}$ was 1.4–1.6. At the distance from $x/D_p = 7D_p$, a gentle scour pit was formed between $x/D_p = 3D_p$ and $x/D_p = 5D_p$, and $\frac{\varepsilon_{tmax,q}}{\varepsilon_m}$ was approximately 1.5–1.7. According to Hamill, the maximum scour depth near the quay wall can be calculated using Equation (10).

$$\frac{\varepsilon_{tmax,q}}{\varepsilon_m} = 1.18\left(\frac{x}{X_m}\right)^{-0.2} \tag{10}$$

The maximum scour depth (X_m) of the twin propellers and the distance between the propeller and sand bed did not satisfy Equation (11) proposed by Hamill. In this study, the axial distance divided by the propeller diameter is dimensionless, i.e., the axial distance was expressed as x/D_p.

$$X_m = {F_0}^{0.94}C \tag{11}$$

For the quay wall at an infinite distance, it can be considered that the quay wall could not influence the scour of the twin propellers. The empirical coefficient of the twin-propeller scour was derived by Cui et al. [31], in which the quay wall was assumed to be infinitely far away from the twin-propeller. The ratio of the maximum scour depth of the twin-propeller to the unlimited scour depth of the single propeller ($\frac{\varepsilon_{tmax,q}}{\varepsilon_m}$) should be 1.2 for ICRTP and 1.1 for ECRTP. In this study, the total length of the flume was 1.2 m, and the free diffusion distance downstream of the propeller $x/D_p > 15$, which could be considered as an unlimited scouring condition. Based on the test data and the above assumptions,

the relationship between the maximum scour depth of the twin propellers near the quay wall, and the axial distance was established (Figure 8). The maximum scour depth of the twin propellers near the quay wall could be predicted simply. The internal propeller was predicted using Equation (12), and the external propeller was predicted using Equation (13).

$$\frac{\varepsilon_{tmax,q}}{\varepsilon_m} = 3.5\frac{x}{D_P}^{-0.4} \tag{12}$$

$$\frac{\varepsilon_{tmax,q}}{\varepsilon_m} = 2.7\frac{x}{D_P}^{-0.35} \tag{13}$$

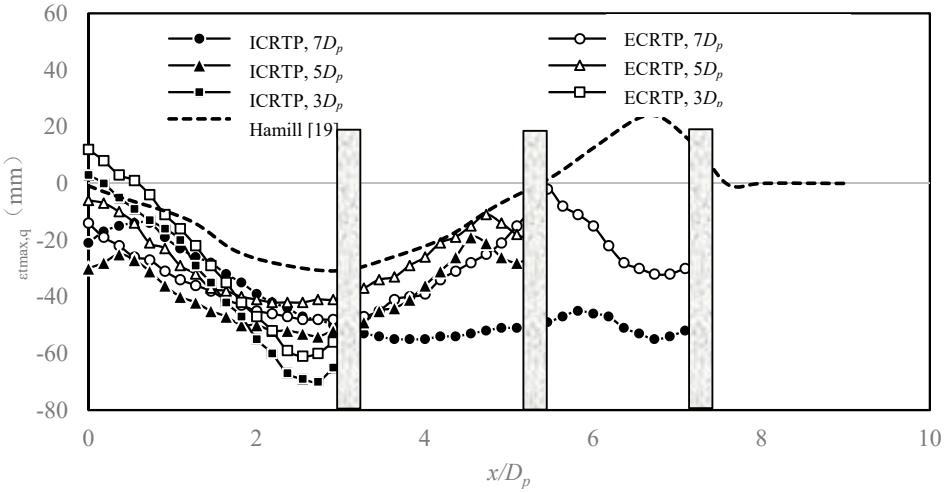

Figure 7. Comparison of maximum scour depth of axis.

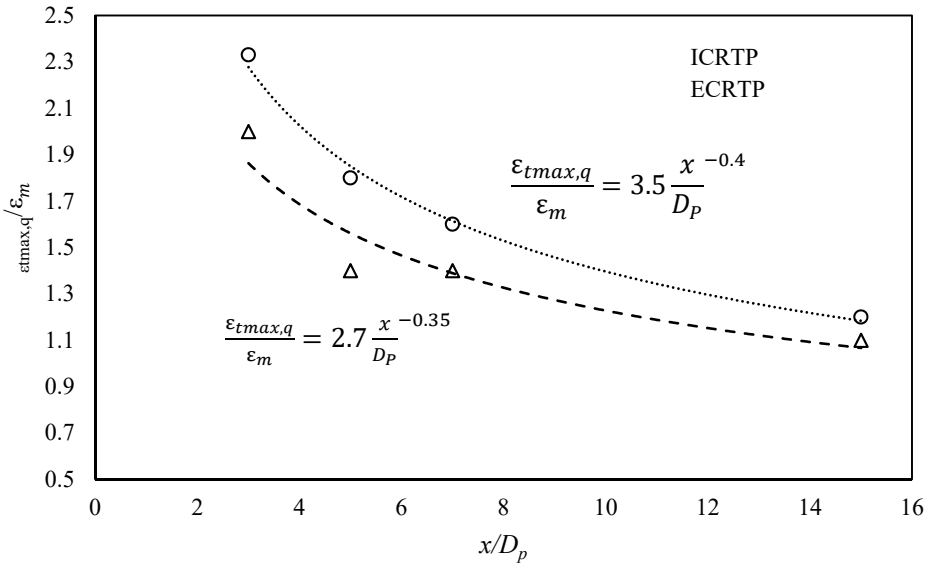

Figure 8. Prediction equation of maximum scour depth of twin propellers near quay wall.

The practical application of the prediction formula proposed in this study is compared with the empirical formula proposed by predecessors. According to the prediction formula (Equation (10)) proposed by Hamill, the maximum scour depth near the quay wall is related to the distance between propeller and quay wall. The proposed formula proposed by Ryan et al. [32] takes the Froude number into account, as Equation (14). Yuksel et al. [33] added the gap of the propeller (G) to these factors,

as shown in Equation (15). Take $5D_p$ spacing as a comparative case, the comparison between the calculated results and the experimental results are shown in Figure 9. Hamill et al. [19], Ryan et al. [32], and Yuksel et al. [33] studied the scour depth of a single propeller near the quay wall. This study is aimed at the scour of twin propellers. The maximum scour depth is much higher than that of a single propeller. The maximum variation is 49%, which occurs in the case of ICRTP with a $3D_p$ spacing.

$$\frac{\varepsilon_{tmax,q}}{\varepsilon_m} = 1.217Fr^{-0.019}\left(\frac{x}{D_P}\right)^{-0.4} \tag{14}$$

$$\frac{\varepsilon_{tmax,q}}{D_P} = 0.512{F_0}^{2.27}\left(\frac{G}{d_{50}}\right)^{-0.65}\left(\frac{x}{D_P}\right)^{-0.543} \tag{15}$$

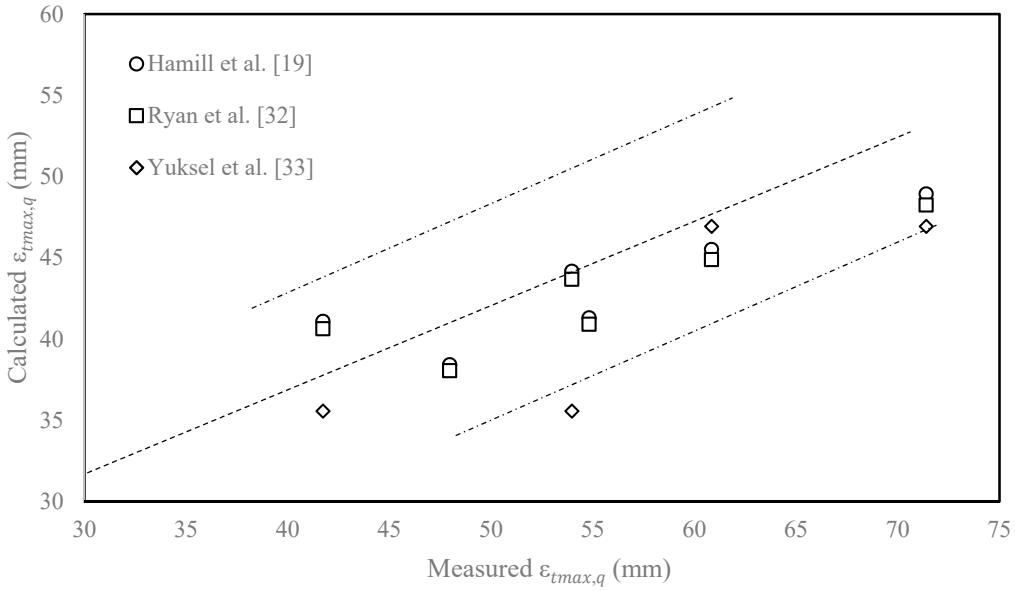

Figure 9. Comparison between the calculated results and the experimental results

4.2. Scour Patterns with Existence of Quay Wall

Cui et al. [31] extensively investigated the scour structure of internal and external rotating twin propellers without considering a quay wall. In general, the scour structure can be defined based on six characteristic parameters: maximum scour depth, maximum scour depth location, maximum scour width, length of main scour pit, maximum deposition height, and maximum deposition position. Based on 1–6 groups of test data, the relationships of the six characteristic parameters between the external and internal rotating twin propellers at $3D_p$, $5D_p$, and $7D_p$ away from the quay wall were analyzed (Tables 4–6).

Table 4. Comparison of scour structures of ECRTP and ICRTP at $3D_p$.

Characteristics of Scour Structure	ECRTP			ICRTP		
	Measurement		Depth–Position Relationship	Measurement		Depth–Position Relationship
	No Quay Wall	Quay Wall		No Quay Wall	Quay Wall	
$\varepsilon_{max,q}$, $\varepsilon_{tmax,e}$, $\varepsilon_{tmax,i}$, (mm)	39	61	$\varepsilon_{tmax,q} = 1.56\ \varepsilon_{max,e}$	42.5	70	$\varepsilon_{tmax,q} = 1.68\ \varepsilon_{max,i}$
X_m, $X_{tm,e}$, $X_{tm,i}$, (m)	0.14	$3D_p$	Near the quay wall	0.13	$3D_p$	Near the quay wall
W_m, $W_{tm,e}$, $W_{tm,i}$, (m)	0.35	0.65	$W_{m,q} = 1.86\ W_{tm,e}$	0.31	0.63	$W_{m,q} = 2.03W_{tm,i}$
X_S, $X_{tS,e}$, $X_{tS,i}$, (m)	0.24	$3D_p$	Near the quay wall	0.28	$3D_p$	Near the quay wall
Z_D, $Z_{tD,e}$, $Z_{tD,i}$, (mm)	32	33	$Z_{tD,q} = 1.03\ Z_{tD,e}$	25	33	$Z_{tD,q} = 1.32\ Z_{tD,i}$
X_D, $X_{tD,e}$, $X_{tD,i}$, (m)	0.32	$5D_p$	Local scour zone	0.37	$4.5D_p$	Local scour zone

Table 5. Comparison of scour structures of external and internal rotating propellers at $5D_p$ away from quay wall.

Characteristics of Scour Structure	ECRTP			ICRTP		
	Measurement		Depth–Position Relationship	Measurement		Depth–Position Relationship
	No Quay Wall	Quay Wall		No Quay Wall	Quay Wall	
$\varepsilon_{max,q}$, $\varepsilon_{tmax,e}$, $\varepsilon_{tmax,i}$, (mm)	39	42	$\varepsilon_{tmax,q} = 1.07\ \varepsilon_{max,e}$	42.5	54	$\varepsilon_{tmax,q} = 1.27\ \varepsilon_{max,i}$
$X_{m,q}$, $X_{tm,e}$, $X_{tm,i}$, (m)	0.14	$2.5D_p$	Main scour hole	0.13	$2.5D_p$	Main scour hole
$W_{m,q}$, $W_{tm,e}$, $W_{tm,i}$, (m)	0.35	0.53	$W_{tm,q} = 1.5\ W_{m,e}$	0.31	0.58	$W_{tm,q} = 1.87W_{m,i}$
$X_{S,q}$, $X_{tS,e}$, $X_{tS,i}$, (m)	0.24	$5D_p$	Near the quay wall	0.28	$5D_p$	Near the quay wall
$Z_{D,q}$, $Z_{tD,e}$, $Z_{tD,i}$, (mm)	32	33	$Z_{tD,Q} = 1.03\ Z0_{tD,i}$	25	38	$Z_{tD,Q} = 1.52\ Z_{tD,I}$
$X_{D,q}$, $X_{tD,e}$, $X_{tD,i}$, (m)	0.32	$3D_p$	Local scour zone	0.37	$4.5D_p$	Local scour zone

Table 6. Comparison of scour structures of external and internal rotating propellers at $7D_p$ away from quay wall.

Characteristics of Scour Structure	ECRTP			ICRTP		
	Measurement		Depth–Position Relationship	Measurement		Depth–Position Relationship
	No Quay Wall	Quay Wall		No Quay Wall	Quay Wall	
$\varepsilon_{max,q}$, $\varepsilon_{tmax,e}$, $\varepsilon_{tmax,i}$, (mm)	39	48	$\varepsilon_{tmax,q} = 1.23\ \varepsilon_{max,e}$	42.5	55	$\varepsilon_{tmax,q} = 1.29\ \varepsilon_{max,i}$
$X_{m,q}$, $X_{tm,e}$, $X_{tm,i}$, (m)	0.14	$2.7D_p$	Main scour hole	0.13	$3.5D_p$	Main scour hole
$W_{m,q}$, $W_{tm,e}$, $W_{tm,i}$, (m)	0.35	0.55	$W_{tm,q} = 1.57\ W_{m,e}$	0.31	0.57	$W_{tm,q} = 1.84W_{m,i}$
$X_{S,q}$, $X_{tS,e}$, $X_{tS,i}$, (m)	0.24	$7D_p$	Near the quay wall	0.28	$7D_p$	Near the quay wall
$Z_{D,q}$, $Z_{tD,e}$, $Z_{tD,i}$, (mm)	32	33	$Z_{tD,Q} = 1.03\ Z0_{tD,i}$	25	28	$Z_{tD,Q} = 1.12\ Z_{tD,I}$
$X_{D,q}$, $X_{tD,e}$, $X_{tD,i}$, (m)	0.32	$3D_p$	$X = 3.5D_p$	0.37	$3.5D_p$	$X = 5.5D_p$

Among the characteristics were the maximum scour depth ($\varepsilon_{tmax,\,q}$ is the maximum scour depth influenced by the quay wall; $\varepsilon_{tmax,\,e}$ is the ECRTP without considering the quay wall effect; $\varepsilon_{tmax,\,i}$ is the ICRTP without considering the quay wall effect), the position of the maximum scour depth ($X_{m,q}$ is the location of the maximum scour depth influenced by the quay wall; $X_{tm,\,e}$ is the ECRTP without considering the quay wall effect; $X_{tm,\,i}$ is the ICRTP without considering the quay wall effect), the maximum scour width ($W_{m,\,q}$ is the maximum scour width affected by the quay wall; $W_{tm,\,e}$ is the ECRTP without considering the quay wall effect; $W_{tm,\,i}$ is the ICRTP without considering the effect of the quay wall), the length of the main scour pit ($X_{S,q}$ is the length of the main scour pit influenced by the quay wall; $X_{tS,e}$ is the ECRTP without considering the quay wall influence; $X_{tS,i}$ is the ICRTP without considering the quay wall effect), the height of deposition ($Z_{D,q}$ is the maximum deposition height considering the quay wall; $Z_{tD,e}$ is the ECRTP without considering the quay wall effect; $Z_{tD,i}$ is the ICRTP without considering the quay wall effect), and the position of the maximum deposition height ($X_{D,q}$ is the maximum deposition position influenced by the quay wall; $X_{tD,e}$ is ECRTP without considering the quay wall; $X_{tD,i}$ is the ICRTP without considering the effect of the quay wall).

The maximum scour depth of twin-propeller proposed in this study can play a guiding role in practical engineering. It mainly includes two methods; one is to control the distance between propeller and quay wall structure. According to the original structure design of the port, the maximum scour depth of the structure is predicted. The safe distance between the ship propeller and the port structure can be deduced. The other method is it is necessary to consider the maximum scour damage that may occur when the ship berths. So that increases the foundation depth of quay wall, or lays a protective layer near the port. The reinforcement depth of quay wall can refer to Equations (12) and (13) proposed in this study. It is worth noting that there is a limitation of this study. When a ship is entering or leaving a port, it is a dynamic process with a low velocity so that the distance between the propellers and the quay wall is constantly changing. This study is not suitable for ships entering and leaving the port at low speed. Because the scour hole is moving when the ship is sailing, it is applicable to the case of ships berthing at the port.

5. Conclusions

In this study, an experimental investigation on the scour of twin propellers was conducted. In a static water tank, a PVC plastic plate was used to simulate a vertical quay wall. Based on the position relationship between the propeller and the vertical quay wall when a ship enters and leaves the

port, three distances and two rotation modes of the propeller were adopted, and the scour of the twin-propeller near the quay wall was determined. The structure could be divided into small scour pits, main scour pits, and local scour zones near the quay wall.

The conclusions of this study are drawn as follows.

1. The scour pattern of twin propellers near the quay wall was different from that of the free scour without the restriction of the quay wall. The axial position of the maximum scour depth was found in the middle of the main scour pit or the quay wall, and the transverse position was related to the rotation state of the propeller. The maximum scour depth of the external twin-propeller was found on the propeller axis, and the internal propeller was found on the central axis.
2. The formation process of the twin-propeller scour influenced by the quay wall could be divided into three stages: (1) Axial scour formation stage, which occurred from the commencement of scouring to the diffusion of the jet to the vertical quay wall. The twin-propeller jet diffused along the axial direction, and the jet transported sand particles on the sand bed surface downstream. The duration of the process was influenced by the distance between the twin-propeller and quay wall. (2) Obstructed scour expansion stage, where the horizontal development stage of the brush area occurred. Near the quay wall, the jet diffused on the quay wall, and the jet continued to carry the sand particles near the quay wall to both sides. This process lasted for a long time from the beginning of the jet diffusion to the quay wall until the scour pit stopped expanding significantly. (3) Equilibrium stage, which the jet diffused in the plane of the quay wall and formed a vortex at the junction between the sand bed and quay wall. The vortex pushed sand particles backward to the inclined surface of the sand bed in the local scour zone and acted under gravity. In addition, the scour structure was in dynamic equilibrium.
3. Based on the different distances between the propeller and quay wall, the quantitative relationships of six characteristic parameters of the scour pit were established. The characteristics were the maximum scour depth, maximum scour depth position, maximum scour width, length of main scour pit, maximum deposition height, and location of maximum deposition height. It was found that the maximum scour depth at $3D_p$ was the highest value, which signified a maximum increase of 70%. Furthermore, it is recommended that the close contact between the propeller and quay wall should be prevented.

Author Contributions: W.H.L.'s long term research series in ship propeller jet induced scour; Y.C. and W.H.L. wrote the manuscript with revisions, recommendations and validations from W.H.L., Z.C.O., L.L., C.L.S., D.R. and G.H. All authors have read and agreed to the published version of the manuscript.

Funding: This research was funded by the Natural Science Foundation of Tianjin City: 18JCYBJC21900 and Science Fund for Creative Research Groups of the National Natural Science Foundation of China (Grant no. 51621092). The APC was funded by the Natural Science Foundation of Tianjin City: 18JCYBJC21900.

Acknowledgments: The authors wish to extend their gratitude to the School of Civil Engineering at Tianjin University for laboratory space; Queen's University Belfast, University of Plymouth, University of Oxford, Dalian University of Technology, University of Malaya (HIR ENG47), Universiti Teknologi Malaysia, and Southern University College for their past support; and professional bodies EI, IEI, IET, IEM, IEAust, ASCE, ECUK, SCUK, BEM, FEANI, AFEO, MINDS and academy AAET for membership support and available resources.

Conflicts of Interest: The authors declare no conflict of interest.

Notation

C = clearance distance from the propeller tip to the sand bed
C_t = thrust coefficient
D_p = propeller diameter
d_p = distance between twin-propellers
d_{50} = average sediment grain size
F_0 = densiometric Froude number
t = time

$\varepsilon_{max,q}$ = depth of maximum scour around the quay wall
$\varepsilon_{tmax,e}$ = depth of maximum scour of external twin-propeller
$\varepsilon_{tmax,i}$ = depth of maximum scour of internal twin-propeller
V_0 = efflux velocity
$W_{m,q}$ = maximum scour width around the quay wall
$W_{tm,e}$ = maximum scour width for external twin-propeller
$W_{tm,i}$ = maximum scour width for internal twin-propeller
$X_{m,q}$ = position of maximum scour depth around the quay wall
$X_{tm,e}$ = position of maximum scour depth for external twin-propeller
$X_{tm,i}$ = position of maximum scour depth for internal twin-propeller
$X_{S,q}$ = length of main scour hole around the quay wall
$X_{tS,e}$ = length of main scour hole for external twin-propeller
$X_{tS,i}$ = length of main scour hole for internal twin-propeller
$X_{D,q}$ = position of maximum deposition height around the quay wall
$X_{tD,e}$ = position of maximum deposition height for external twin-propeller
$X_{tD,i}$ = position of maximum deposition height for internal twin-propeller
$Z_{D,q}$ = maximum deposition height around the quay wall
$Z_{tD,e}$ = maximum deposition height of external twin-propeller
$Z_{tD,i}$ = maximum deposition height of internal twin-propeller

References

1. Albertson, M.L.; Dai, Y.B.; Jensen, R.A.; Rouse, H. *Diffusion of Submerged Jets*; American Society of Civil Engineers: Reston, VA, USA, 1950; Volume 115, pp. 639–664.
2. Blaauw, H.G.; van de Kaa, E.J. *Scour of Bottom and Sloping Banks Caused by the Screw Race of the Manoeuvring Ships*; Delft Hydraulics Laboratory: Delft, The Netherlands, 1978; Rep. No. 202.
3. Berger, W.; Felkel, K.; Hager, M.; Oebius, H.; Schale, E. Courant provoque par les bateaux protection des berges et solutionpour eviterl'scour du lit du haut rhin. In Proceedings of the 25th PIANC Congress, Edinburgh, Scotland, May 1981.
4. Verhey, H.J.; Blockland, T.; Bogaerts, M.P.; Volger, D.; Weyde, R.W. Experiences in Netherlands with quay structures subjected to velocities created by bow thrusters and main propellers of mooring and unmooring ships. In *Bulletin de l'Association Internationale Permanente des Congrès de Navigation*; Permanent International Association of Navigation Congresses: Bruxelles, Belgium, 1987; Volume 58, pp. 69–88.
5. Hamill, G.A. Characteristics of the Screw Wash of a Manoeuvring Ship and the Resulting Bed Scour. Ph.D. Thesis, Queen's University of Belfast, Belfast, UK, 1987.
6. Lam, W.H. Simulations of a Ship's Propeller Jet. Ph.D. Thesis, Queen's University of Belfast, Belfast, UK, 2008.
7. Du, G. *Research on Hydrodynamic Performance of Wheel Drive Propeller*; Harbin Engineering University: Harbin, China, 2017.
8. Su, Y.M.; Chi TG, S.; Jia, F.S. Numerical analysis of the wake field of ship propeller. *Ocean Eng.* **2002**, *3*, 44–48.
9. Hong, F.W.; Zhang, Z.R.; Liu, D.C.; Zhen, C.S. Numerical analysis of flow field and hydrodynamic force of ship propeller. *Hydrodyn. Res. Prog. Part A* **2020**, *35*, 68–73.
10. Jiang, J.X.; Lam, W.H.; Cui, Y.G.; Zhang, T.M.; Sun, C.; Guo, J.H.; Ma, Y.B.; Wang, S.G.; Hamill, G. Ship Twin-propeller Jet Model used to Predict the Initial Velocity and Velocity Distribution within Diffusing Jet. *KSCE J. Civil Eng.* **2018**, *23*, 1118–1131. [CrossRef]
11. BAW (Bundesanstalt für Wasserbau). *Principles for the Design of Bank and Bottom Protection for Inland Waterway*; BAW: Karlsruhe, Germany, 2010.
12. PIANC. *Guidelines for Protecting Berthing Structures from Scour Caused by Ships. Report no.180*; The World Association for Waterborne Transportation Infrastructure: Brussels, Belgium, 2015.
13. Bergh, H.; Cederwall, K. *Propeller Scour in Harbours. Bulletin No TRITA-VBI-107*; Hydraulics Laboratory, Royal Institute of Technology: Stockholm, Sweden, 1981.
14. Bergh, H.; Magnusson, N. Propeller scour and protection methods used in ferry terminals in the port of Stockholm. In Proceedings of the Permanent International Association of Navigation Congresses, Stockholm, Sweden, 2–6 July 1987; Volume 58, pp. 112–120.

15. Verhey, H.J. Stability of Bottom and Banks Subjected to the Velocities in the Propeller Jet Behind Ships. In Proceedings of the International Harbour Congress, 8th, Antwerp, Belgium, 13–17 June 1983.
16. Stewart, D.P.; Hamill, G.A.; Johnston, H.T. Bed scour considerations in ship berth design. In Proceedings of the International Conference on Coastal and Port Engineering in Developing Countries, Mombasa, Kenya, 16–20 September 1991; pp. 1110–1125.
17. Kim, Y.G.; Kim, S.Y.; Kim, H.T.; Lee, S.K.; Yu, B.S. Prediction of the manoeuvrability of a large container ship with twin-propeller and twin rudders. *Mar. Sci. Technol.* **2007**, *12*, 130–138. [CrossRef]
18. McGarvey, J.A. The Influence of the Rudder on the Hydrodynamics and the Resulting Bed Scour, of a Ship's Screw Wash. Ph.D. Thesis, Queen's University of Belfast, Belfast, UK, 1996.
19. Hamill, G.A.; Johnston, H.T.; Stewart, D.P. Propeller wash scour near quay walls. *J. Waterw. Port Coast.* **1999**, *125*, 170–175. [CrossRef]
20. Wei, M.; Chiew, Y. Influence of Toe Clearance on Propeller Scour around an Open-Type Quay. *J. Hydraul. Eng.* **2017**, *143*, 4017012. [CrossRef]
21. Hong, J.H.; Chiew, Y.M.; Cheng, N.S. Scour Caused by a Propeller Jet. *J. Hydraul. Eng.* **2013**, *139*, 1003–1012. [CrossRef]
22. Wei, M.; Chiew, Y.; Guan, D. Temporal Development of Propeller Scour around a Sloping Bank. *J. Waterw. Port Coast. Ocean Eng.* **2018**, *144*, 6018005. [CrossRef]
23. Tan, R.; Yüksel, Y. Seabed scour induced by a propeller jet. *Ocean Eng.* **2018**, *160*, 132–142. [CrossRef]
24. Cui, Y.; Lam, W.; Zhang, T.; Sun, C.; Robinson, D.; Hamill, G. Temporal Model for Ship Twin-Propeller Jet Induced Sandbed Scour. *J. Mar. Sci. Eng.* **2019**, *7*, 339. [CrossRef]
25. Mujal-Colilles, A.; Castells, M.; Llull, T.; Gironella, X.; Martínez de Osés, X. Stern Twin-Propeller Effects on Harbor Infrastructures. Experimental Analysis. *Water* **2018**, *10*, 1571. [CrossRef]
26. Yuksel, Y.; Tan, R.I.; Celikoglu, Y. Propeller jet flow scour around a pile structure. *Appl. Ocean Res.* **2018**, *79*, 160–172. [CrossRef]
27. Yew, W.T. Seabed Scour Induced by Twin-Propeller Ships. Ph.D. Thesis, University of Malaya, Kuala Lumpur, Malaysia, 2017.
28. Li, Y.; Ong, M.C.; Fuhrman, D.R.; Larsen, B.E. Numerical investigation of wave-plus-current induced scour beneath two submarine pipelines in tandem. *Coast. Eng.* **2020**, *156*, 103619. [CrossRef]
29. Ong, M.C.; Utnes, T.; Holmedal, L.E.; Myrhaug, D.; Pettersen, B. Numerical simulation of flow around a circular cylinder close to a flat seabed at high Reynolds numbers using a k–ε model. *Coast. Eng.* **2010**, *57*, 931–947. [CrossRef]
30. Cui, Y.; Lam, W.; Zhang, T.; Sun, C.; Hamill, G. Scour Induced by Single and Twin Propeller Jets. *Water* **2019**, *11*, 1097. [CrossRef]
31. Cui, Y.; Lam, W.; Robinson, D.; Hamill, G. Temporal and spatial scour caused by external and internal counter-rotating twin-propellers using Acoustic Doppler Velocimetry. *Appl. Ocean Res.* **2020**, *97*. [CrossRef]
32. Ryan, D.; Hamill, G.A. Determining Propeller Erosion at the Stern of a Berthing Ship. *J. Waterw. Port Coast. Ocean Eng.* **2013**, *139*, 247–255. [CrossRef]
33. Yuksel, Y.; Tan, R.I.; Celikoglu, Y. Determining propeller scour near a quay wall. *Ocean Eng.* **2019**, *188*, 106331. [CrossRef]